A second-order BGK scheme for the equations of radiation hydrodynamics [*]

Song Jiang   Wenjun Sun

LCP, Institute of Applied Physics and Computational Mathematics,
P.O. Box 8009, Beijing 100088, China.

E-mail: jiang@iapcm.ac.cn,   sun_wenjun@iacpm.ac.cn

Abstract

We present a second-order BGK scheme for the equations of multidimensional radiation hydrodynamics (RHE) in zero diffusion limit by using the generalized Maxwellian in [1] and the second-order BGK scheme for the Euler equations in [2, 3]. This extends a (first-order) kinetic flux vector splitting scheme (KFVS) for RHE in [1] to a second-order BGK scheme. Several one- and two-dimensional numerical examples demonstrate improvement of the scheme in accuracy and resolution compared with the KFVS scheme in [1] and the first-order BGK scheme.

Keywords: Radiation hydrodynamics, zero diffusion, 2nd-order BGK scheme, KFVS scheme.

1   Introduction

In this paper, we present a second-order BGK scheme for the equations of multidimensional radiation hydrodynamics in zero diffusion limit.

The importance of thermal radiation in physical problems increases as the temperature is raised. At moderate temperatures, the role of the radiation is primarily one of transporting energy by radiative process, while at higher temperature, the energy and momentum densities of the radiation field may become comparable to or even dominates the corresponding fluid quantities. In this case, the radiation field significantly affects the dynamics of the fluid. Hydrodynamics with explicit account of the radiation energy and momentum contributions constitutes the charter of "radiation hydrodynamics". The theory of radiation hydrodynamics finds a wide range of application, including such diverse astrophysical phenomena as waves and oscillations in stellar atmospheres and envelopes, nonlinear stellar pulsation, supernova explosions, stellar winds, and many others (see, e.g., [4–6]). It has also direct application in other areas, for example to the physics of laser fusion and of reentry vehicles.

In the case of (equilibrium diffusion and) zero diffusion limit, the equations of radiation hydrodynamics can be written as a nonlinear hyperbolic system of conservation laws, but different from the Euler equations in the (high nonlinear) radiation terms. In numerical simulations of radiation hydrodynamics, one of the main difficulties (of standard numerical methods) is to

resolve and keep track of strong shocks. Dai and Woodward [7] proposed the Godunov scheme inclusive of linear and nonlinear Riemann solvers for the equations of radiation hydrodynamics. Their numerical results show that their scheme preserves the principle advantages of Godunov schemes. However, to our knowledge, their method is relatively costly.

In the past years, the development of the gas-kinetic schemes, such as kinetic flux vector splitting schemes (KFVS) based on the collisionless Boltzmann equation (see, e.g., [1, 8–13]) and BGK scheme based on a collisional BGK model (see, e.g., [2, 14–16]), has attracted much attention and significant progress has been made. These gas-kinetic schemes do not require any Riemann solvers, and they have provided robust and accurate numerical solutions for various unsteady compressible flow (for example, cf. [11, 12, 15, 16] and the reference therein). For the equations of radiation hydrodynamics in zero diffusion limit, Tang and Wu [1] constructed a KFVS scheme, and presented several numerical examples to demonstrate the performance of their scheme. As is well-known, the BGK schemes differ from the KFVS-type schemes mainly on the inclusion of particle collisions in the gas evolution stage. Instead of solving the collisionless Boltzmann equation, the BGK schemes use a collisional BGK model in the numerical flux evaluation. Since the gas evolution process is a relaxation process from a nonequilibrium state to an equilibrium one, the entropy condition is always satisfied by the BGK scheme. Moreover, due to its specific governing equation, the BGK scheme gives the compressible Navier-Stokes equations in smooth regions, and provides a delicate dissipative mechanism, which is controlled by the pseudo-particle collision time and the intrinsic collisional model, to get a stable and crisp shock transition in nonsmooth regions.

In this paper, we propose a second-order BGK scheme for the equations of multidimensional radiation hydrodynamics in zero diffusion limit by including the non-equilibrium effect to a KFVS scheme, and hence, extend the first-order KFVS scheme in [1] to a second-order BGK scheme. This extension to the second-order is the contribution of the present paper. To construct our scheme, we use a generalized Maxwellian distribution introduced in [1] to recover the radiation hydrodynamical equations, and then, to apply the second-order BGK scheme for the Euler equations described in [2, 3] to simulate and keep track of strong shocks, thus resulting in a second-order BGK scheme for the multidimensional radiation hydrodynamics in zero diffusion limit. The numerical tests show an obvious improvement in accuracy and resolution of the scheme of this paper over the scheme proposed in [1] and the first-order BGK scheme.

This paper is organized as follows: In Section 2, we recall the macroscopic description of radiation hydrodynamics and the gas distribution function of equilibrium states in [1] to recover the $d-$dimensional radiation hydrodynamical equations in zero diffusion limit. In Section 3, the second-order BGK scheme is presented based on the generalized Maxwellian distribution given in Section 2. In section 4, several numerical tests are presented which demonstrate the availablity and accuracy of the present scheme, and comparisons with the KFVS scheme in [1] and the first-order BGK scheme are given.

2   Equations of radiation hydrodynamics in zero diffusion limit

For the equations of radiation hydrodynamics in zero diffusion limit, there are two ways of description, one is macroscopic while the other is microscopic. We first introduce the macroscopic equations describing the motion of a gas under a radiation field. Assuming that the radiative temperature and the fluid temperature are equal, and that the gas is radiatively opaque so that the equilibrium diffusion will be dealt with, and the mean-free-path of photons is much smaller than the typical length of the flow, then, we can write the equations of radiation hydrodynamics without radiative heat-diffusion in $\mathbb{R}^d$, describing the conservation of mass, momentum and

energy, as (cf. [4,5])

$$\begin{cases} \partial_t \rho + \operatorname{div}(\rho \mathbf{u}) = 0, \\[2mm] \partial_t(\rho \mathbf{u}) + \operatorname{div}(\rho \mathbf{u} \otimes \mathbf{u}) + \nabla\left(p + \frac{1}{3}a_R T^4\right) = 0, \\[2mm] \partial_t E + \operatorname{div}\left[\mathbf{u}\left(E + p + \frac{1}{3}a_R T^4\right)\right] = 0, \end{cases} \tag{2.1}$$

where ρ, $\mathbf{u} = (u_1, \cdots, u_d)$, p and T denote the density, velocity, flow pressure and absolute temperature, respectively, $a_R > 0$ is a radiation constant, and

$$E = \frac{1}{2}\rho \mathbf{u}^2 + \rho e + a_R T^4 \tag{2.2}$$

is the total energy, $e = e(\rho, T)$ is the internal energy, $\mathbf{u}^2 = u_1^2 + \cdots + u_d^2$.

From (2.1) and (2.2) we see that the system includes both gas and radiative contributions to flow dynamics. The quantities $\frac{1}{3}a_R T^4$ and $a_R T^4$ represent the radiative pressure and radiative energy density, respectively. To complete the system (2.1), one needs the equation of state for the pressure $p = p(\rho, T)$. In this paper for the purpose of our test problems, we will limit our study to the polytropic ideal gas: $p = (\gamma - 1)\rho e$ with $\gamma > 1$ being the specific heat ratio and $e = c_v T$ with c_v being the specific heat, and as in [1,7], we assume $c_v = 1$ without loss of generality. We point out that if one assumes $a_R = 0$ in (2.1), then the system (2.1) reduces to the usual inviscid Euler equations.

Another way to describe the flow motion is based on the particle motion, or the statistical description of a fluid, in which a gas distribution function $f(x, t, \mathbf{v})$ is introduced to describe the probability of particles to be located in a certain velocity interval, and to approximate usually the particle number density at a certain velocity in hydrodynamics, where $\mathbf{v} = (v_1, \cdots, v_d)$ is the particle velocity. Usually, the distribution function f is a basic unknown in the kinetic theory, and satisfies the Boltzmann equation, we refer to [17, 18]) for the theory on the Boltzmann equation.

The thermodynamic aspect of gas dynamics is based on the assumption that the deviation of a gas from a local equilibrium state is sufficiently small. The distribution function f is usually unknown in the real flow situation. However, the distribution function g corresponding to a local equilibrium state can be explicitly given if the mass, momentum and energy are known. The gas distribution function for an equilibrium state plays an important role in the construction of gas-kinetic schemes. In the sequel, we study the equilibrium distribution for (2.1).

For the system (2.1) with $a_R = 0$, i.e. the Euler equations with γ-law, the equilibrium state is the Maxwellian distribution (cf. [17, 18]),

$$g(x, t, \mathbf{v}, \xi) = \rho\left(\frac{\lambda}{\pi}\right)^{(d+K)/2} e^{-\lambda[(\mathbf{v}-\mathbf{u})^2 + \xi^2]}, \tag{2.3}$$

where $\xi^2 = \xi_1^2 + \cdots + \xi_K^2$, $(\mathbf{v} - \mathbf{u})^2 = (v_1 - u_1)^2 + \cdots + (v_d - u_d)^2$, and $K = -d + 2/(\gamma - 1)$ is the internal degree of freedom, $\lambda = m/2kT$ with k and m being the molecular mass and the Boltzmann constant respectively. Actually, $K = 1$ in the numerical tests of this paper because $d = 2$ and $\gamma = 5/3$ are chosen. Then, the Euler equations can be recovered by taking moments as

$$\int_{\mathbb{R}^d \times \mathbb{R}^K} \psi\left(\partial_t g + \mathbf{v} \cdot \nabla g\right) d\Xi = 0, \tag{2.4}$$

where and *in what follows*, $d\Xi = dv_1 \cdots dv_d d\xi_1 \cdots d\xi_K$, and the vector function ψ is given by

$$\psi = \left(1, v_1, \cdots, v_d, \frac{v^2 + \xi^2}{2}\right)^t,$$

and the superscript ^{t} denotes transposition.

On the other hand, when $a_R \neq 0$, the system (2.1) can not (easily) be written in the moment form (2.4) through a Maxwellian distribution. As in [1], here we introduce an equilibrium state function with two parameters λ_1 and λ_2, instead of one parameter λ, to recover (2.1) by the moment method. Hence, we modify the Maxwellian distribution g in (2.3) to

$$\bar{g}(x, t, \mathbf{v}, \xi) = \rho \left(\frac{\lambda_1}{\pi}\right)^{d/2} \left(\frac{\lambda_2}{\pi}\right)^{K/2} e^{-\lambda_1 (\mathbf{v} - \mathbf{u})^2 - \lambda_2 \xi^2}, \tag{2.5}$$

where λ_1 and λ_2 are functions of T, m and k, and will be determined below.

Now, if we take moments of ψ with $\bar{g}$, we obtain

$$\begin{pmatrix} \rho \\ \\ \rho u_i \\ \\ \frac{1}{2}\left(\rho \mathbf{u}^2 + d\frac{\rho}{2\lambda_1} + K\frac{\rho}{2\lambda_2}\right) \end{pmatrix} = \int_{\mathbb{R}^d \times \mathbb{R}^K} \psi \bar{g} \, d\Xi \tag{2.6}$$

and

$$\begin{pmatrix} \rho u_j \\ \\ \rho u_i u_j + \frac{\rho}{2\lambda_1}\delta_{ij} \\ \\ \frac{1}{2} u_j \left[\rho \mathbf{u}^2 + (d+2)\frac{\rho}{2\lambda_1} + K\frac{\rho}{2\lambda_2}\right] \end{pmatrix} = \int_{\mathbb{R}^d \times \mathbb{R}^K} v_j \psi \bar{g} \, d\Xi, \tag{2.7}$$

where $d\Xi = dv_1 \cdots dv_d d\xi_1 \cdots d\xi_K$.

Comparing (2.6) and (2.7) with (2.1), we easily see that in order to recover the system (2.1) by taking the moments of the distribution $\bar{g}$, the parameters λ_1 and λ_2 have to satisfy

$$\begin{cases} \dfrac{\rho}{2\lambda_1} = p + \dfrac{1}{3} a_R T^4, \\ K\dfrac{\rho}{2\lambda_2} = Kp + \left(2 - \dfrac{d}{3}\right) a_R T^4. \end{cases} \tag{2.8}$$

We will use the modified Maxwellian (2.5) to construct our second-order BGK scheme in the next section.

3 A 2nd-order BGK scheme based on the generalized Maxwellian

Using the Maxwellian distribution (2.5), Tang and Wu [1] proposed a KFVS algorithm of first-order for the system (2.1) based on the relations (2.6)–(2.8). In this section, based on the generalized Maxwellian distribution $\bar{g}$ given in (2.5) and the BGK schemes described in [2,3], we construct a second-order BGK scheme for the system (2.1), therefore, extending the KFVS scheme of first-order in [1].

For simplicity, we only describe our scheme for (2.1) in two dimensions. Extension to three-dimensional problems is straightforward. We use (U, V) to denote the velocity components (u_1, u_2) in the x- and y-directions, and write (2.1) as

$$\frac{\partial W}{\partial t} + \frac{\partial F(W)}{\partial x} + \frac{\partial G(W)}{\partial y} = 0, \tag{3.1}$$

where

$$W = (\rho, \rho U, \rho V, E)^t,$$

$$F(W) = \left(\rho U, \rho U^2 + p + \frac{a_R}{3} T^4, \rho UV, U(E + p + \frac{a_R}{3} T^4) \right)^t,$$

$$G(W) = \left(\rho V, \rho UV, \rho V^2 + p + \frac{a_R}{3} T^4, V(E + p + \frac{a_R}{3} T^4) \right)^t.$$

Let $x_i = i\Delta x$, $y_j = j\Delta y$ and $t^n = n\Delta t$ $(i, j, n \in \mathbb{Z})$ be the uniform mesh in cartesian coordinates, where the $\Delta x, \Delta y$ and Δt are the mesh sizes in the x-, y- and t-directions, respectively; and let (i, j) denote the cell $\{(x, y); \ x_{i-1/2} < x < x_{i+1/2}, y_{i-1/2} < y < y_{i+1/2}\}$, where $x_{i-1/2} = (i - \frac{1}{2})\Delta x$ and $y_{i-1/2} = (i - \frac{1}{2})\Delta y$.

We denote by

$$W_{i,j} = (\rho_{i,j}, (\rho U)_{i,j}, (\rho V)_{i,j}, E_{i,j}) \tag{3.2}$$

the cell averaged conservative variables at time t^n in cell (i, j) whose center is $(x_{i,j}, y_{i,j})$.

Upon integrating the system (3.1) over the cell (i, j) and $(t^n, t^n + \Delta t)$, a conservative numerical scheme for (3.1) is of the form

$$W_{i,j}^{n+1} = W_{i,j} + \frac{1}{\Delta x} \int_{t^n}^{t^n + \Delta t} (F_{i-1/2,j} - F_{i+1/2,j}) dt + \frac{1}{\Delta y} \int_{t^n}^{t^n + \Delta t} (G_{i,j-1/2} - G_{i,j+1/2}) dt, \tag{3.3}$$

where $F_{i-1/2,j}$ and $G_{i,j-1/2}$ are the time-dependent numerical fluxes in the x- and y-directions across the cell interface.

A BGK scheme is to construct the numerical fluxes $F_{i-1/2,j}$, $G_{i,j-1/2}$ by means of the explicit solution of the BKG model and the relations between the macroscopic variables and the gas distribution function (the solution of the BGK model). In this paper, we use the BGK model to construct $F_{i-1/2,j}$, $G_{i,j-1/2}$ of second order by including the non-equilibrium effect, and give therefore a second-order BGK scheme for (3.1).

The construction of the numerical fluxes $F_{i-1/2,j}$, $G_{i,j-1/2}$ is mainly divided in two stages: (1) *Initial reconstruction.* It is directly applied to the initial cell-averaged conservative variables to get the interpolated values (piecewise linear function) by using limiters. (2) *Gas evolution stage.* It is a process to get the solution of the governing equation with the initial data obtained from the first stage. More precisely, one can construct the initial distribution function f_0 and the equilibrium state $\bar{g}$ from the reconstructed initial data, and thus obtain the general explicit solution (3.26) (i.e. (3.7)) of the BGK model at cell interfaces, from which one gets the numerical flux across cell interfaces. In the sequel we will describe the stages in details.

The BGK model in two dimensions reads:

$$f_t + uf_x + vf_y = -\frac{f - \bar{g}}{\tau}, \tag{3.4}$$

where (u, v) is the particle velocity, τ is the particle collision time related to the viscosity and heat conduction coefficients, and $\bar{g}$ is the Maxwellian distribution given by (2.5) that should satisfy the compatibility condition:

$$\int (f - \bar{g}) \psi \, du dv d\xi = 0, \tag{3.5}$$

5

where

$$\psi = (\psi_1, \psi_2, \psi_3, \psi_4)^t \equiv \left(1, u, v, \frac{1}{2}(u^2 + v^2 + \xi^2)\right)^t$$

are the invariants. Recall that both f and $\bar{g}$ depend on x, t, u, v and ξ.

Stage I. Initial Reconstruction. For a high resolution scheme, reconstruction techniques are usually used to interpolate the cell averaged mass, momentum and energy densities. The standard nonlinear limiter, in particular the MUSCL limiter [19] is used in this paper.

Denote by

$$W_{i,j} = (\rho_{i,j}, (\rho U)_{i,j}, (\rho V)_{i,j}, E_{i,j})$$

the cell averaged initial conservative variables in cell (i, j) whose center is $(x_{i,j}, y_{i,j})$, where (U, V) denotes the flow velocity. The initial flow variables are constructed as

$$\bar{W}_{i,j}(x, y) = W_{i,j} + L_x(W)(x - x_{i,j}) + L_y(W)(y - y_{i,j}), \tag{3.6}$$

where the slopes $L_x(W), L_y(W)$ are defined as follows: Let the function

$$L(s_+, s_-) = (\mathrm{sign}(s_+) + \mathrm{sign}(s_-)) \min\left\{2|s_+|, 2|s_-|, \frac{1}{2}|s_+ + s_-|\right\}$$

be the MUSCL limiter [19], then the slopes $L_x(W)$ and $L_y(W)$ take the form

$$L_x(W) = L\left(\frac{W_{i+1,j} - W_{i,j}}{x_{i+1,j} - x_{i,j}}, \frac{W_{i,j} - W_{i-1,j}}{x_{i,j} - x_{i-1,j}}\right),$$

and

$$L_y(W) = L\left(\frac{W_{i,j+1} - W_{i,j}}{x_{i,j+1} - x_{i,j}}, \frac{W_{i,j} - W_{i,j-1}}{x_{i,j} - x_{i,j-1}}\right).$$

Stage II. Gas Evolution. In the evolution stage, we utilize the explicit solution of the BGK model (3.4). Denote the cell interface between cells (i, j) and $(i + 1, j)$ by $\Gamma_{i+1/2,j} = \{(x_{i+1/2,j}, y); \ j - \frac{1}{2} \le y \le j + \frac{1}{2}\}$. The general solution f of (3.4) at the point $X_{ij} = (x_{i+1/2,j}, y_{i+1/2,j}) \in \Gamma_{i+1/2,j}$ and time t is given by

$$f(X_{ij}, t, u, v, \xi) = \frac{1}{\tau} \int_0^t \bar{g}(x', y', t', u, v, \xi) e^{-(t-t')/\tau} dt'$$
$$+ e^{-t/\tau} f_0(x_{i+1/2,j} - ut, y_{i+1/2,j} - vt), \tag{3.7}$$

where $x' = x_{i+1/2,j} - u(t - t')$, $y' = y_{i+1/2,j} - v(t - t')$, f_0 is the initial gas distribution function.

For simplicity, we assume $x_{i+1/2,j} = 0$, $y_{i+1/2,j} = 0$. The initial gas distribution function f_0 is assumed to have the form

$$f_0(x, y) = \begin{cases} g_l(1 + a_l x + b_l y), & x < 0, \\ g_r(1 + a_r x + b_r y), & x > 0, \end{cases} \tag{3.8}$$

with g_l, g_r being the Maxwellian distributions at the left and right of the cell interface which, in view of (2.5), have the general form

$$g_l = \rho_l \frac{\lambda_{1l}}{\pi} \left(\frac{\lambda_{2l}}{\pi}\right)^{K/2} e^{-\lambda_{1l}[(u-U_l)^2 + (v-V_l)^2] - \lambda_{2l}\xi^2},$$

and

$$g_r = \rho_r \frac{\lambda_{1r}}{\pi} \left(\frac{\lambda_{2r}}{\pi}\right)^{K/2} e^{-\lambda_{1r}[(u-U_r)^2 + (v-V_r)^2] - \lambda_{2r}\xi^2}.$$

6

The representation (3.8) means that even with a discontinuity at the cell interface, the gas is assumed to stay in an equilibrium state on both sides of discontinuity, see [20] for more details.

The terms a_l, b_l, a_r, b_r in (3.8) are related to the spatial derivatives of a Maxwellian, and assumed to have the following form obtained from the Taylor expansion of the Maxwellian (2.5) (cf. (3.16)):

$$\begin{cases} a_l = a_{1l} + a_{2l}u + a_{3l}v + \frac{1}{2}a_{4l}(u^2 + v^2) + \frac{1}{2}a_{5l}\xi^2, \\[2mm] b_l = b_{1l} + b_{2l}u + b_{3l}v + \frac{1}{2}b_{4l}(u^2 + v^2) + \frac{1}{2}b_{5l}\xi^2, \\[2mm] a_r = a_{1r} + a_{2r}u + a_{3r}v + \frac{1}{2}a_{4r}(u^2 + v^2) + \frac{1}{2}a_{5r}\xi^2, \\[2mm] b_r = b_{1r} + b_{2r}u + b_{3r}v + \frac{1}{2}b_{4r}(u^2 + v^2) + \frac{1}{2}b_{5r}\xi^2. \end{cases} \tag{3.9}$$

Let $\bar{W}(x,y)$ be the piecewise linear function whose restriction on the cell (i,j) is $\bar{W}_{i,j}(x,y)$. Then, from the following relation between the macroscopic variables $\bar{W}$ and the gas distribution function f_0 (cf. (2.6))

$$\bar{W} = \int \psi f_0 \, du\, dv\, d\xi, \tag{3.10}$$

we can obtain both g_l and g_r as well as their slopes in (3.8). In fact, by the initial reconstruction (3.6), the left and right macroscopic states at the point $X_{ij} = (x_{i+1/2,j}, y_{i+1/2,j}) \in \Gamma_{i+1/2,j}$ are

$$\bar{W}_{i,j}(X_{ij}) = \begin{pmatrix} \bar{\rho}_{i,j}(X_{ij}) \\ (\bar{\rho}\bar{U})_{i,j}(X_{ij}) \\ (\bar{\rho}\bar{V})_{i,j}(X_{ij}) \\ \bar{E}_{i,j}(X_{ij}) \end{pmatrix}, \quad \bar{W}_{i+1,j}(X_{ij}) = \begin{pmatrix} \bar{\rho}_{i+1,j}(X_{ij}) \\ (\bar{\rho}\bar{U})_{i+1,j}(X_{ij}) \\ (\bar{\rho}\bar{V})_{i+1,j}(X_{ij}) \\ \bar{E}_{i+1,j}(X_{ij}) \end{pmatrix}, \tag{3.11}$$

which imply that

$$\begin{pmatrix} \rho_l \\ U_l \\ V_l \end{pmatrix} = \begin{pmatrix} \bar{\rho}_{i,j}(X_{ij}) \\ \bar{U}_{i,j}(X_{ij}) \\ \bar{V}_{i,j}(X_{ij}) \end{pmatrix}, \quad \begin{pmatrix} \rho_r \\ U_r \\ V_r \end{pmatrix} = \begin{pmatrix} \bar{\rho}_{i+1,j}(X_{ij}) \\ \bar{U}_{i+1,j}(X_{ij}) \\ \bar{V}_{i+1,j}(X_{ij}) \end{pmatrix}.$$

Correspondingly, $\lambda_{1l}, \lambda_{2l}, \lambda_{1r}, \lambda_{2r}$ satisfy

$$\begin{cases} \dfrac{\bar{\rho}_{i,j}(X_{ij})}{2\lambda_{1l}} = \bar{p}_{i,j}(X_{ij}) + \dfrac{1}{3}a_R\bar{T}_{i,j}^4(X_{ij}), \\[4mm] K\dfrac{\bar{\rho}_{i,j}(X_{ij})}{2\lambda_{2l}} = K\bar{p}_{i,j}(X_{ij}) + \left(2 - \dfrac{d}{3}\right)a_R\bar{T}_{i,j}^4(X_{ij}). \end{cases}$$

and

$$\begin{cases} \dfrac{\bar{\rho}_{i+1,j}(X_{ij})}{2\lambda_{1r}} = \bar{p}_{i+1,j}(X_{ij}) + \dfrac{1}{3}a_R\bar{T}_{i+1,j}^4(X_{ij}), \\[4mm] K\dfrac{\bar{\rho}_{i+1,j}(X_{ij})}{2\lambda_{2r}} = K\bar{p}_{i+1,j}(X_{ij}) + \left(2 - \dfrac{d}{3}\right)a_R\bar{T}_{i+1,j}^4(X_{ij}), \end{cases}$$

where we have used $\bar{p}_{i,j}, \bar{T}^4_{i,j}$ and $\bar{p}_{i+1,j}, \bar{T}^4_{i+1,j}$ to denote the values of the pressure p and the temperature T in the left and right cells of the point $X_{ij} \in \Gamma_{1+1/2,j}$.

On the other hand, if we differentiate (3.10) with respect to x and y, and take into account (3.6), (3.8) and (3.9), we see that a_l and b_l can be obtained by the relations:

$$\frac{1}{\rho_l}L_x = \frac{1}{\rho_l}\begin{pmatrix}(\partial\rho/\partial x)_l \\ (\partial(\rho U)/\partial x)_l \\ (\partial(\rho V)/\partial x)_l \\ (\partial E/\partial x)_l\end{pmatrix} = \frac{1}{\rho_l}\int \psi a_l g_l du dv d\xi = M_l \begin{pmatrix}a_{1l} \\ a_{2l} \\ a_{3l} \\ a_{4l} \\ a_{5l}\end{pmatrix}, \qquad (3.12)$$

and

$$\frac{1}{\rho_l}L_y = \frac{1}{\rho_l}\begin{pmatrix}(\partial\rho/\partial y)_l \\ (\partial(\rho U)/\partial y)_l \\ (\partial(\rho V)/\partial y)_l \\ (\partial E/\partial y)_l\end{pmatrix} = \frac{1}{\rho_l}\int \psi b_l g_l du dv d\xi = M_l \begin{pmatrix}b_{1l} \\ b_{2l} \\ b_{3l} \\ b_{4l} \\ b_{5l}\end{pmatrix}. \qquad (3.13)$$

The matrix

$$M_l = \frac{1}{\rho_l}\int \psi \otimes \widetilde{\psi} g_l du dv d\xi$$

is a function of the parameters $(U_l, V_l, \lambda_{1l}, \lambda_{2l})$ in g_l, having the following form

$$M_l = \begin{pmatrix} 1 & U_l & V_l & \mathcal{B}_1 - \frac{K}{4\lambda_{2l}} & \frac{K}{4\lambda_{2l}} \\ U_l & U_l^2 + \frac{1}{2\lambda_{1l}} & U_l V_l & \mathcal{B}_2 - \frac{KU_l}{4\lambda_{2l}} & \frac{KU_l}{4\lambda_{2l}} \\ V_l & U_l V_l & V_l^2 + \frac{1}{2\lambda_{1l}} & \mathcal{B}_3 - \frac{KV_l}{4\lambda_{2l}} & \frac{KV_l}{4\lambda_{2l}} \\ \mathcal{B}_1 & \mathcal{B}_2 & \mathcal{B}_3 & \mathcal{B}_4 & \mathcal{B}_5 \end{pmatrix}, \qquad (3.14)$$

where

$$\widetilde{\psi} = (1, u, v, \tfrac{1}{2}(u^2 + v^2), \tfrac{1}{2}\xi^2)^t,$$

$$\mathcal{B}_1 = \tfrac{1}{2}\left(U_l^2 + V_l^2 + \tfrac{1}{\lambda_{1l}} + \tfrac{K}{2}\tfrac{1}{\lambda_{2l}}\right),$$

$$\mathcal{B}_2 = \tfrac{1}{2}\left(U_l^3 + V_l^2 U_l + 2\tfrac{U_l}{\lambda_{1l}} + \tfrac{K}{2}\tfrac{U_l}{\lambda_{2l}}\right),$$

$$\mathcal{B}_3 = \tfrac{1}{2}\left(V_l^3 + U_l^2 V_l + 2\tfrac{V_l}{\lambda_{1l}} + \tfrac{K}{2}\tfrac{V_l}{\lambda_{2l}}\right),$$

$$\mathcal{B}_4 = \tfrac{1}{4}\left((U_l^2 + V_l^2)^2 + (\tfrac{4}{\lambda_{1l}} + \tfrac{K}{2\lambda_{2l}})(U_l^2 + V_l^2) + \tfrac{3}{2\lambda_{1l}^2} + \tfrac{2K+2}{4\lambda_{1l}\lambda_{2l}}\right),$$

$$\mathcal{B}_5 = \tfrac{1}{4}\left(\tfrac{K}{2\lambda_{2l}}(U_l^2 + V_l^2) + \tfrac{K(K+2)}{4\lambda_{2l}^2} + \tfrac{K}{2\lambda_{1l}\lambda_{2l}}\right).$$

In order to complete the equations (3.12) and (3.13), one has to give an additional equation for $\vec{a}_l = (a_{1l}, \cdots, a_{5l})$ and $\vec{b}_l = (b_{1l}, \cdots, b_{5l})$ respectively. In fact, recalling (3.8) and (3.9), the direct Taylor expansion of the Maxwellian (2.5) upon the spatial variables x and y leads to

$$a_{1l} = \frac{1}{\rho_l}\left(\frac{\partial\rho}{\partial x}\right)_l + \frac{d}{2\lambda_{1l}}\left(\frac{\partial\lambda_1}{\partial x}\right)_l + \frac{K}{2\lambda_{2l}}\left(\frac{\partial\lambda_2}{\partial x}\right)_l - \left(\frac{\partial}{\partial x}\left[\lambda_1(U^2 + V^2)\right]\right)_l,$$

$$a_{2l} = 2\left(\frac{\partial(\lambda_1 U)}{\partial x}\right)_l, \quad a_{3l} = 2\left(\frac{\partial(\lambda_1 V)}{\partial x}\right)_l, \quad a_{4l} = -2\left(\frac{\partial\lambda_1}{\partial x}\right)_l, \quad a_{5l} = -2\left(\frac{\partial\lambda_2}{\partial x}\right)_l,$$

$$b_{1l} = \frac{1}{\rho_l}\left(\frac{\partial\rho}{\partial y}\right)_l + \frac{d}{2\lambda_{1l}}\left(\frac{\partial\lambda_1}{\partial y}\right)_l + \frac{K}{2\lambda_{2l}}\left(\frac{\partial\lambda_2}{\partial y}\right)_l - \left(\frac{\partial}{\partial y}\left[\lambda_1(U^2 + V^2)\right]\right)_l,$$

$$b_{2l} = 2\left(\frac{\partial(\lambda_1 U)}{\partial y}\right)_l, \quad b_{3l} = 2\left(\frac{\partial(\lambda_1 V)}{\partial y}\right)_l, \quad b_{4l} = -2\left(\frac{\partial\lambda_1}{\partial y}\right)_l, \quad b_{5l} = -2\left(\frac{\partial\lambda_2}{\partial y}\right)_l. \tag{3.16}$$

Eliminating T^4 in the relations (2.8) and differentiating then the resulting equation with respect to x and y, we obtain

$$\frac{K\rho_l}{12\lambda_{2l}^2}a_{5l} - \frac{(2-d/3)\rho_l}{4\lambda_{1l}^2}a_{4l} = \left(\frac{(2-d/3)}{2\lambda_{1l}} - \frac{K}{6\lambda_{2l}}\right)\left(\frac{\partial\rho}{\partial x}\right)_l - \left(2 - \frac{d}{3} - \frac{K}{3}\right)\left(\frac{\partial p}{\partial x}\right)_l,$$

$$\frac{K\rho_l}{12\lambda_{2l}^2}b_{5l} - \frac{(2-d/3)\rho_l}{4\lambda_{1l}^2}b_{4l} = \left(\frac{(2-d/3)}{2\lambda_{1l}} - \frac{K}{6\lambda_{2l}}\right)\left(\frac{\partial\rho}{\partial y}\right)_l - \left(2 - \frac{d}{3} - \frac{K}{3}\right)\left(\frac{\partial p}{\partial y}\right)_l, \tag{3.17}$$

where (by (2.2))

$$\left(\frac{\partial p}{\partial x}\right)_l = (\gamma - 1)\left(T_l\left(\frac{\partial\rho}{\partial x}\right)_l + \rho_l\left(\frac{\partial T}{\partial x}\right)_l\right),$$

$$\left(\frac{\partial T}{\partial x}\right)_l = (\rho_l + 4a_R T_l^3)^{-1}\left\{\left(\frac{\partial E}{\partial x}\right)_l - \rho_l U_l\left(\frac{\partial U}{\partial x}\right)_l - \rho_l V_l\left(\frac{\partial V}{\partial x}\right)_l - \frac{1}{2}\left(U_l^2 + V_l^2\right)\left(\frac{\partial\rho}{\partial x}\right)_l - T_l\left(\frac{\partial\rho}{\partial x}\right)_l\right\},$$

and $\frac{\partial p_l}{\partial y}$ is given in the same manner. Thus, solving the system of algebraic equations (3.12), (3.13) and (3.17), one obtains a_l and b_l. In the same manner, the slopes a_r and b_r can be obtained. So, in view of (3.8), the initial distribution f_0 has been determined.

To determine the equilibrium state $\bar{g}$ in (3.4) around the point $(x = 0, y = 0)$ of the cell interface, we assume that $\bar{g}$ is given by

$$\bar{g}(x, y, t) = g_0(1 + \bar{a}_l x(1 - H(x)) + \bar{a}_r x H(x) + \bar{b}y + \bar{A}t), \tag{3.18}$$

where $H(x)$ is the Heaviside function, g_0 is a local Maxwellian distribution located at $(x = y = 0, t = 0)$. Notice that $\bar{g}$ is continuous but has different x-slopes on both sides of $x = 0$.

The local Maxwellian distribution g_0 has the form (cf. (2.5))

$$g_0 = \frac{\lambda_{10}}{\pi}\left(\frac{\lambda_{20}}{\pi}\right)^{K/2} e^{-\lambda_{10}[(u-U_0)^2 + (v-V_0)^2] - \lambda_{20}\xi^2}, \tag{3.19}$$

where U_0, V_0, λ_{10} and λ_{20} (at time $t = 0$) can be obtained as follows, using (3.7) with $t \to 0$, and the compatibility condition (3.5) at $(x = y = 0, t = 0)$ and taking into account (2.6).

$$W_0 \equiv \begin{pmatrix} \rho_0 \\ \rho_0 U_0 \\ \rho_0 V_0 \\ E_0 \end{pmatrix} = \int \psi g_0 du dv d\xi = \int_{u>0}\int \psi g_l du dv d\xi + \int_{u<0}\int \psi g_r du dv d\xi, \tag{3.20}$$

9

which gives W_0. Once the macroscopic variables W_0 is obtained, the parameters λ_{10} and λ_{20} are then given by

$$\frac{\rho_0}{2\lambda_{10}} = p_0 + \frac{1}{3}a_R T_0^4, \qquad K\frac{\rho}{2\lambda_{20}} = Kp_0 + \left(2 - \frac{d}{3}\right)a_R T_0^4. \tag{3.21}$$

From (3.20) and (3.21), we get $U_0, V_0, \lambda_{10}, \lambda_{20}$. Thus, g_0 is determined.

As aforementioned, the coefficients $\bar{a}_l, \bar{a}_r, \bar{b}, \bar{A}$ in $\bar{g}$ are related to the derivatives of a Maxwellian in space and time, and assumed to have the following form obtained from a Taylor expansion of a Maxwellian,

$$\bar{a}_l = \bar{a}_{1l} + \bar{a}_{2l}u + \bar{a}_{3l}v + \frac{1}{2}\bar{a}_{4l}(u^2 + v^2) + \frac{1}{2}\bar{a}_{5l}\xi^2,$$

$$\bar{a}_r = \bar{a}_{1r} + \bar{a}_{2r}u + \bar{a}_{3r}v + \frac{1}{2}\bar{a}_{4r}(u^2 + v^2) + \frac{1}{2}\bar{a}_{5r}\xi^2,$$

$$\bar{b} = \bar{b}_1 + \bar{b}_2 u + \bar{b}_3 v + \frac{1}{2}\bar{b}_4(u^2 + v^2) + \frac{1}{2}\bar{b}_5\xi^2,$$

$$\bar{A} = \bar{A}_1 + \bar{A}_2 u + \bar{A}_3 v + \frac{1}{2}\bar{A}_4(u^2 + v^2) + \frac{1}{2}\bar{A}_5\xi^2.$$

Then, $\bar{a}_l, \bar{a}_r$ in $\bar{g}$ can be obtained by differentiating (3.5) with respect to x, and taking then the value at $(x = y = 0, t = 0)$ as follows (cf. the derivation of (3.12)).

$$\frac{W_0 - \bar{W}_{i,j}(x_{i,j}, y_{i,j})}{\rho_0 \Delta x^-} = \bar{M}_0 \begin{pmatrix} \bar{a}_{1l} \\ \bar{a}_{2l} \\ \bar{a}_{3l} \\ \bar{a}_{4l} \\ \bar{a}_{5l} \end{pmatrix}, \qquad -\frac{W_0 - \bar{W}_{i+1,j}(x_{i+1,j}, y_{i+1,j})}{\rho_0 \Delta x^+} = \bar{M}_0 \begin{pmatrix} \bar{a}_{1r} \\ \bar{a}_{2r} \\ \bar{a}_{3r} \\ \bar{a}_{4r} \\ \bar{a}_{5r} \end{pmatrix},$$

where $\Delta x^- = x_{i+1/2} - x_i$, $\Delta x^+ = x_{i+1} - x_{i+1/2}$; and the matrix $\bar{M}_0 = \frac{1}{\rho_0}\int \psi \otimes \tilde{\psi} g_0 du dv d\xi$ has the same structure as the matrix M_l only with $\rho_l, U_l, V_l, \lambda_{1l}$ and λ_{2l} replaced by $\rho_0, U_0, V_0, \bar{\lambda}_{10}$ and $\bar{\lambda}_{20}$. On the other hand, there should hold

$$\frac{K\rho_0}{12\lambda_{20}^2}\bar{a}_{5l} - \frac{(2-d/3)\rho_0}{4\lambda_{10}^2}\bar{a}_{4l} = \left(\frac{(2-d/3)}{2\lambda_{10}} - \frac{K}{6\lambda_{20}}\right)\overline{\left(\frac{\partial \rho_0}{\partial x}\right)}_l - \left(2 - \frac{d}{3} - \frac{K}{3}\right)\overline{\left(\frac{\partial p_0}{\partial x}\right)}_l,$$

$$\frac{K\rho_0}{12\lambda_{20}^2}\bar{a}_{5r} - \frac{(2-d/3)\rho_0}{4\lambda_{10}^2}\bar{a}_{4r} = \left(\frac{(2-d/3)}{2\lambda_{10}} - \frac{K}{6\lambda_{20}}\right)\overline{\left(\frac{\partial \rho_0}{\partial x}\right)}_r - \left(2 - \frac{d}{3} - \frac{K}{3}\right)\overline{\left(\frac{\partial p_0}{\partial x}\right)}_r,$$

where we denote

$$\left(\overline{\left(\frac{\partial \rho_0}{\partial x}\right)}_l, \overline{\left(\frac{\partial(\rho_0 U_0)}{\partial x}\right)}_l, \overline{\left(\frac{\partial(\rho_0 V_0)}{\partial x}\right)}_l, \overline{\left(\frac{\partial E_0}{\partial x}\right)}_l \right) = \left(\frac{W_0 - \bar{W}_{i,j}(x_{i,j}, y_{i,j})}{\rho_0 \Delta x^-}\right)^t,$$

$$\left(\overline{\left(\frac{\partial \rho_0}{\partial x}\right)}_r, \overline{\left(\frac{\partial(\rho_0 U_0)}{\partial x}\right)}_r, \overline{\left(\frac{\partial(\rho_0 V_0)}{\partial x}\right)}_r, \overline{\left(\frac{\partial E_0}{\partial x}\right)}_r \right) = \left(-\frac{W_0 - \bar{W}_{i+1,j}(x_{i+1,j}, y_{i+1,j})}{\rho_0 \Delta x^+}\right)^t,$$

$$\overline{\left(\frac{\partial p_0}{\partial x}\right)}_l = (\gamma - 1)\left(T_0 \overline{\left(\frac{\partial \rho_0}{\partial x}\right)}_l + \rho_0 \overline{\left(\frac{\partial T_0}{\partial x}\right)}_l\right),$$

$$\overline{\left(\frac{\partial T_0}{\partial x}\right)}_l = (\rho_0 + 4a_R T_0^3)^{-1}\left\{\overline{\left(\frac{\partial E_0}{\partial x}\right)}_l - T_0\overline{\left(\frac{\partial \rho_0}{\partial x}\right)}_l - \rho_0 U_0 \overline{\left(\frac{\partial U_0}{\partial x}\right)}_l - \rho_0 V_0 \overline{\left(\frac{\partial V_0}{\partial x}\right)}_l - \frac{1}{2}(U_0^2 + V_0^2)\overline{\left(\frac{\partial \rho_0}{\partial x}\right)}_l\right\},$$

and $(\frac{\overline{\partial p_0}}{\partial x})_r$ is defined in the same manner.

In the y-direction at $(x = y = 0, t = 0)$, the term $\bar{b}$ in $\bar{g}$ can be determined by the compatibility condition,

$$\frac{\partial}{\partial y} \int \psi(g - f_0) du dv d\xi = 0,$$

which yields consequently

$$\frac{1}{\rho_0} \int \psi \bar{b} g_0 du dv d\xi = \bar{M}_0 \begin{pmatrix} \bar{b}_1 \\ \bar{b}_2 \\ \bar{b}_3 \\ \bar{b}_4 \\ \bar{b}_5 \end{pmatrix} = \frac{1}{\rho_0} \Big(\int_{u>0} \int \psi b_l g_l du dv d\xi + \int_{u<0} \int \psi b_r g_r du dv d\xi \Big).$$

Similarly, b_4, b_5 should satisfy

$$\frac{K\rho_0}{12\lambda_{20}^2} \bar{b}_5 - \frac{(2-d/3)\rho_0}{4\lambda_{10}^2} \bar{b}_4 = \Big(\frac{(2-d/3)}{2\lambda_{10}} - \frac{K}{6\lambda_{20}} \Big) (\frac{\overline{\partial \rho_0}}{\partial y})_0 - (2 - \frac{d}{3} - \frac{K}{3}) (\frac{\overline{\partial p_0}}{\partial y})_0,$$

where we denote

$$\Big((\frac{\overline{\partial \rho_0}}{\partial y})_0, (\frac{\overline{\partial(\rho_0 U_0)}}{\partial y})_0, (\frac{\overline{\partial(\rho_0 V_0)}}{\partial y})_0, (\frac{\overline{\partial E_0}}{\partial y})_0 \Big) = \frac{1}{\rho_0} \Big(\int_{u>0} \int \psi b_l g_l du dv d\xi + \int_{u<0} \int \psi b_r g_r du dv d\xi \Big)^t,$$

$$(\frac{\overline{\partial p_0}}{\partial y})_0 = (\gamma - 1) \Big(T_0 (\frac{\overline{\partial \rho_0}}{\partial y})_0 + \rho_0 (\frac{\overline{\partial T_0}}{\partial y})_0 \Big),$$

$$(\frac{\overline{\partial T_0}}{\partial y})_0 = (\rho_0 + 4a_R T_0^3)^{-1} \Big\{ (\frac{\overline{\partial E_0}}{\partial y})_0 - T_0 (\frac{\overline{\partial \rho_0}}{\partial y})_0 - \rho_0 U_0 (\frac{\overline{\partial U_0}}{\partial y})_0 - \rho_0 V_0 (\frac{\overline{\partial V_0}}{\partial y})_0 - \frac{1}{2} (U_0^2 + V_0^2) (\frac{\overline{\partial \rho_0}}{\partial y})_0 \Big\}.$$

Solving the above algebraic equations, one gets the coefficient $\bar{b}$.

Up to now, we have determined all the parameters in the initial gas distribution function f_0 and the equilibrium state $\bar{g}$ at the beginning of the each time step $t = 0$. Inserting (3.8) and (3.18) into the equation (3.7), we obtain the final gas distribution function $f(x, y, t, u, v)$ at the point $x = y = 0$,

$$f(0, 0, t, u, v, \xi) = (1 - e^{-t/\tau}) g_0 + (\tau(-1 + e^{-t/\tau}) + t e^{-t/\tau}) \Big[\Big(\bar{a}_l H(u) + \bar{a}_r (1 - H(u)) \Big) u + \bar{b} v \Big] g_0$$

$$+ \tau \Big(\frac{t}{\tau} - 1 + e^{-t/\tau} \Big) \bar{A} g_0$$

$$+ e^{-t/\tau} \Big[(1 - u t a_l - v t b_l) H(u) g_l + (1 - u t a_r - v t b_r)(1 - H(u)) g_r \Big], \qquad (3.26)$$

where the only unknown left is $\bar{A}$. To determine $\bar{A}$, we use the compatibility condition (3.5) at $x = y = 0$ in the whole time step Δt, namely

$$\int_0^{\Delta t} \int (\bar{g} - f)(0, 0, t, u, v, \xi) \psi du dv d\xi dt = 0,$$

which yields

$$\bar{M}_0 \bar{A} = \frac{1}{\rho_0} \int \Big\{ \gamma_1 g_0 + \gamma_2 u[\bar{a}_l H(u) + \bar{a}_r (1 - H(u)) + \bar{b} v] + \gamma_3 [H(u) g_l + (1 - H(u)) g_r]$$

$$+ \gamma_4 u[(a_l u + b_l v) H(u) g_l + (a_r u + b_r v)(1 - H(u)) g_r] \Big\} \psi du dv d\xi, \qquad (3.27)$$

where

$$\gamma_0 = \Delta - \tau(1 - e^{-\Delta/\tau}),$$
$$\gamma_1 = -(1 - e^{-\Delta t/\tau})/\gamma_0,$$
$$\gamma_2 = [-\Delta t + 2\tau(1 - e^{-\Delta/\tau}) - \Delta t e^{-\Delta t/\tau}]/\gamma_0,$$
$$\gamma_3 = (1 - e^{-\Delta t/\tau})/\gamma_0,$$
$$\gamma_4 = [\Delta t e^{-\Delta t/\tau} - \tau(1 - e^{-\Delta t/\tau})]/\gamma_0.$$

Since all the moments on the right hand side of the equation (3.27) can be calculated explicitly, if we denote that

$$\left((\overline{\tfrac{\partial \rho_0}{\partial t}}), (\overline{\tfrac{\partial(\rho_0 U_0)}{\partial t}}), (\overline{\tfrac{\partial(\rho_0 V_0)}{\partial t}}), (\overline{\tfrac{\partial E_0}{\partial t}}) \right) = (\text{ the right hand side of (3.27) })^t,$$

$$(\overline{\tfrac{\partial p_0}{\partial t}}) = (\gamma - 1)\left(T_0(\overline{\tfrac{\partial \rho_0}{\partial t}}) + \rho_0(\overline{\tfrac{\partial T_0}{\partial t}}) \right),$$

$$(\overline{\tfrac{\partial T_0}{\partial t}}) = (\rho_0 + 4a_R T_0^3)^{-1}\left\{ (\overline{\tfrac{\partial E_0}{\partial t}}) - T_0(\overline{\tfrac{\partial \rho_0}{\partial t}}) - \rho_0 U_0(\overline{\tfrac{\partial U_0}{\partial t}}) - \rho_0 V_0(\overline{\tfrac{\partial V_0}{\partial t}}) - \tfrac{1}{2}(U_0^2 + V_0^2)(\overline{\tfrac{\partial \rho_0}{\partial t}}) \right\}.$$

Then $\bar{A}_4$ and $\bar{A}_5$ should satisfy

$$\frac{K\rho_0}{12\lambda_{20}^2}\bar{A}_5 - \frac{(2-d/3)\rho_0}{4\lambda_{10}^2}\bar{A}_4 = \left(\frac{(2-d/3)}{2\lambda_{10}} - \frac{K}{6\lambda_{20}} \right)(\overline{\tfrac{\partial \rho_0}{\partial t}}) - \left(2 - \frac{d}{3} - \frac{K}{3} \right)(\overline{\tfrac{\partial p_0}{\partial t}}).$$

Solving the above algebraic equations, one obtains then the coefficient $\bar{A}$.

Thus, we have obtained all the parameters which are needed in the construction of the gas distribution function $f(x, y, t, u, v, \xi)$ at a cell interface. Once we get f, the time-dependent numerical flux $F_{i+1/2,j}$ from (3.3) in the x-direction across the cell interface is given then by taking the moments of f with the invariants (recalling $x_{i+1/2,j} = 0$):

$$F_{i+1/2,j} = \begin{pmatrix} \mathcal{F}_\rho \\ \mathcal{F}_{\rho U} \\ \mathcal{F}_{\rho V} \\ \mathcal{F}_E \end{pmatrix} = \int u \begin{pmatrix} 1 \\ u \\ v \\ \tfrac{1}{2}(u^2 + v^2 + \xi^2) \end{pmatrix} f(0, 0, t, u, v, \xi) du dv d\xi. \qquad (3.30)$$

In the same manner, we can construct the time-dependent numerical flux $G_{i,j+1/2}$ in the y-direction. Having constructed $F_{i+1/2,j}$ and $G_{i,j+1/2}$, we can get by (3.3) the total mass, momentum and energy at time step t^{n+1}. This procedure can be repeated in the next time level.

In summary, our numerical algorithm consists of two steps:

(1) *Initial reconstruction:* it is directly applied to the conservative variables to get the interpolated values $\bar{W}_{i,j}(x, y)$ from the cell average $W_{i,j}$ by using limiters.

(2) *Gas evolution stage:* it is a process to get the solution of the governing equation with the initial data obtained from the first step. More precisely, one can construct the initial distribution function f_0 and the equilibrium state $\bar{g}$ from the reconstructed initial data, and thus obtain the general explicit solution (3.26) (i.e. (3.7)) of the BGK model at cell interfaces, from which one gets the numerical flux across cell interfaces.

As the end of this section, we point out that due to inclusion of the non-equilibrium effect, the BGK scheme of this paper solves actually the compressible Navier-Stokes equations (3.31)

below, which provide a delicate dissipative mechanism controlled by the pseudo-particle collision time and the intrinsic collisional model, to get a stable and crisp shock transition in nonsmooth regions. In fact, by terms of the Chapman-Enskog expansion and straightforward calculations, we see that the first-order approximation of the BGK model (3.4) is given by

$$
\begin{pmatrix} \rho \\ \rho U \\ \rho V \\ E \end{pmatrix}_t + \begin{pmatrix} \rho U \\ \rho U^2 + P \\ \rho UV \\ (E+P)U \end{pmatrix}_x + \begin{pmatrix} \rho V \\ \rho UV \\ \rho V^2 + P \\ (E+P)V \end{pmatrix}_y = \begin{pmatrix} 0 \\ s_{1x} \\ s_{2x} \\ s_{3x} \end{pmatrix}_x + \begin{pmatrix} 0 \\ s_{1y} \\ s_{2y} \\ s_{3y} \end{pmatrix}_y , \qquad (3.31)
$$

where

$$
P = (\gamma - 1)\rho T + \frac{a_R T^4}{3},
$$

$$
E = \frac{1}{2}(\rho U^2 + \rho V^2) + \rho T + a_R T^4,
$$

$$
s_{1x} = \tau \Big\{ 2PU_x - \Big(\frac{(\gamma-1)\rho + 4a_R T^3/3}{\rho + 4a_R T^3}(P + a_R T^4) - \frac{a_R T^4}{3} \Big)(U_x + V_y) \Big\},
$$

$$
s_{1y} = \tau P(U_x + V_y),
$$

$$
s_{2x} = \tau P(U_x + V_y),
$$

$$
s_{2y} = \tau \Big\{ 2PV_y - \Big(\frac{(\gamma-1)\rho + 4a_R T^3/3}{\rho + 4a_R T^3}(P + a_R T^4) - \frac{a_R T^4}{3} \Big)(V_y + U_x) \Big\},
$$

$$
s_{3x} = \tau \Big\{ P[2UU_x + V(U_y + V_x)] + \Big(\frac{\gamma \rho T + 4a_R T^4/3}{\rho} \Big)_x
$$
$$
- U \Big(\frac{(\gamma-1)\rho + 4a_R T^3/3}{\rho + 4a_R T^3}(P + a_R T^4) - \frac{a_R T^4}{3} \Big)(U_x + V_y) \Big\},
$$

$$
s_{3y} = \tau \Big\{ P[VV_y + U(U_y + V_x)] + \Big(\frac{\gamma \rho T + 4a_R T^4/3}{\rho} \Big)_y
$$
$$
- V \Big(\frac{(\gamma-1)\rho + 4a_R T^3/3}{\rho + 4a_R T^3}(P + a_R T^4) - \frac{a_R T^4}{3} \Big)(U_x + V_y) \Big\}.
$$

From the right-hand side of (3.31), it is not difficult to see that for $1 \leq \gamma \leq 3$ the right-hand side of $(3.31)_2$–$(3.31)_4$ is an elliptic operator with respect to U, V, T, which enhance the stability of the BGK scheme. On the other hand, $\partial_x s_{3x}$ and $\partial_y s_{3y}$ contain the second-order terms ρ_{xx}, ρ_{yy}, the coefficients of which are always non-positive, while for the Euler equations this is not the case because of $a_R = 0$. These negative second-order terms perhaps could affect the stability of the scheme for some problems, and this would be our future study. Fortunately, in our numerical tests given in the next section, we do not observe instability.

4   Numerical tests

In this section, we present some numerical examples, some of which have been tested by the (first-order) KFVS scheme presented in [1] and [7]. To show the performance of our scheme, the comparison with the numerical results in [1] is given.

For all numerical examples in this section, the collision time τ is taken as

$$\tau = \epsilon \Delta t + \min\left\{1.0, C_1 \frac{|P_l - P_r|}{P_l + P_r}\right\}\Delta t, \tag{4.1}$$

where Δt is the CFL time step, and P_l, P_r are the corresponding pressures in the states g_l, g_r of the initial gas distribution function f_0 respectively, ϵ and C_1 are positive constants. In (4.1), the first term on the right hand side gives a limit on the collision time to avoid the blowing up the computation such as the evaluation of $\Delta t/\tau$, and also provides a background dissipation for the numerical fluid, while the second term is related to the pressure jump which introduces additional artificial dissipation if high pressure gradients are present in the fluid. In the smooth flow region or in the vicinity of the slip line, the artificial dissipation introduced is very small or diminishes because of continuous pressure distribution, see [3, 20, 21] for more discussions. We will apply the MUSCL-type limiter to reconstruct the macroscopic initial data, and use uniform grids and take $\gamma = 5/3$ in all numerical tests.

In the following first three examples, we test our scheme for one-dimensional problems, in which we take all $\epsilon = 0.01$, $a_R = 1$, $C_1 = 5.0$ and CFL= 0.45.

Example 1. One-dimensional shock-tube problem with the initial data

$$(\rho, T, u)_{t=0} = \begin{cases} (1, 0.5, 50), & x < 0.6, \\ (2, 1, -40), & x > 0.6. \end{cases}$$

A 100 grid cells with $\Delta x = 0.01$ are employed in the simulation domain $(0, 1)$. Fig.1 shows the numerical results for the total density, temperature and velocity at $t = 0.04$. The results are compared with those of using the KFVS scheme of Tang and Wu [1] and the 1st-order BGK as well as 2000 cells. It can be seen that the 2nd-order BGK scheme resolves obviously better than the KFVS and 1st-order schemes.

Example 2. To show that the scheme does work well with strong shocks, we take the initial data of one-dimensional Riemann problem as

$$(\rho, T, u)_{t=0} = \begin{cases} (1, 0.5, 150), & x < 0.5, \\ (2, 1, -100), & x > 0.5. \end{cases}$$

The computation is performed in the domain $(0, 1)$ with 100 cells ($\Delta x = 0.01$). The simulation results are shown in Fig.2 for the total density, temperature and velocity at $t = 0.018$. We can observe an obvious improvement of the 2nd-order BGK scheme over the KFVS and 1st-order schemes.

Example 3. One-dimensional shock-tube problem involving the rarefaction waves with the initial data for (ρ, T, u):

$$(\rho, T, u)_{t=0} = \begin{cases} (1, 1, -1), & x < 0.5, \\ (1, 1, 1), & x > 0.5. \end{cases}$$

The computation is performed in the domain $(0, 1)$ with 100 cells ($\Delta x = 0.01$). Fig.3 shows the numerical results for the total density, temperature and velocity at $t = 0.2$. We observe that the

results here are comparable to those in [7], and again that the 2nd-order BGK scheme resolves obviously better than the KFVS and 1st-order schemes. We should point out that there is a "starting error" resulting from the purely discontinuous initial data, which induces some error at $x = 0.5$.

In the following two examples, we test our scheme for two-dimensional problems, and we take all $\epsilon = 0.05$, $C_1 = 5.0$ and CFL= 0.45.

Example 4. The first problem is the interaction between a shock and a denser cylindrical bubble. Initially, there is a Mach 256.7 strong shock at $x_0 = 1.64$, propagating in the x-direction. The pre- and post-shock states for (ρ, T, u, v) are taken as (1, 0.01, -22.9472, 0) and (6.57615, 20, 0, 0). On the other hand, there is a cylindrical bubble with radius $R = 0.15$ located at $(x_0 + 0.18, 0.5)$, and the state in the bubble is 100 denser than the pre-shock state. The computation domain is 2×1, the left, right, upper and lower boundary conditions are zero gradient for the flow variables, and $a_R = 0.01$. A grid of 256×128 with $\Delta x = \Delta y = 1/128$ is used in the computation. The numerical results for the density and temperature at $t = 0.07$ are shown in Fig.4, where comparing with the results in [1, 7], good agreement is seen here in the large-scale structure. The comparison of our scheme with the KFVS scheme in [1] is given in Fig.5, where one-dimensional contours are shown. We see that the 2nd-order scheme resolves better in accuracy, comparing with the result obtained using 512 cells.

Example 5. The second problem is the interaction between a wind and a denser cylindrical bubble. Initially, there is a cylindrical bubble of radius $R = 0.15$ with its center located at (0.3,0.5) in the computation domain 2×1. The bubble is 25 times denser than the ambient gas whose state is (1, 0.09, 0, 0) for (ρ, T, u, v). In this problem, the wind is introduced through the left boundary, on which the state $(1, 0.09, 6(1 - e^{-10t}), 0)$ for (ρ, T, u, v) is always assigned. The right, upper and lower boundary conditions are zero gradient for the flow variables, a_R is taken to be 1. The computation is performed with 256×128 cells ($\Delta x = \Delta y = 1/128$). The simulation results for density and temperature at $t = 0.6$ are shown in Fig.6, where the simulated results reproduce the large-scale structure of the corresponding numerical results in [1, 7]. The comparison of our scheme with the KFVS scheme in [1] is given in Fig.7, where one-dimensional contours are shown. Again, we observe from Fig.7 that that the 2nd-order scheme performs better in resolution, comparing with the result obtained using 512 cells.

5 Conclusions

In this paper, based on the inclusion of a non-equilibrium effect to a KFVS scheme, the use of the generalized Maxwellian introduced in [1] and the second-order BGK scheme for the Euler equations in [2,3], we present a second-order BGK scheme for the equations of multidimensional radiation hydrodynamics in (equilibrium diffusion and) zero diffusion limit, and extend therefore the first-order KFVS scheme in [1] to a second-order BGK scheme. One- and two-dimensional numerical experiments are carried out, and the numerical results validate the scheme and show that the 2nd-order BGK scheme improves obviously the accuracy and resolution over the KFVS scheme and the 1st-order BGK scheme.

We should point out that in view of the Chapman-Enskog expansion, the BGK scheme of the present paper solves actually the compressible Navier-Stokes equations (3.31), which provide a delicate dissipative mechanism controlled by the pseudo-particle collision time and the intrinsic collisional model, to get a stable and crisp shock transition in nonsmooth regions. However, the non-positivity of the coefficients of ρ_{xx} and ρ_{yy} on the right-hand side of $(3.31)_4$ could perhaps

affect the stability of the scheme for some problems(although no instability is present in our numerical tests), and this would be the topic of the further studies.

References

[1] Tang, H.Z. and Wu, H.M., *Kinetic flux vector splitting for radiation hydrodynamical equations.* Computers and Fluids **29** (2000), 917-933.

[2] Prendergast, K.H. and Xu K., *Numerical hydrodynamics from gas-kinetic theory.* J. Comput. Phys. **109** 1993), 53-66.

[3] Xu, K., Gas Kinetic Scheme for Unsteady Compressible Flow Simulations. Von Kárman Institute for Fluid Dynamics, Lecture Note Series 1998-03 (1998).

[4] Pomraning, G.C., The Equations of Radiation Hydrodynamics. Oxford: Pergamon Press, 1973.

[5] Castor, J.I., Radiation Hydrodynamics. Cambridge: Cambrige Univ. Press, 2004.

[6] Mihalas, D. and Mihalas, B.W., Foundations of Radiation Hydrodynamics. New York: Oxford University Press, 1984.

[7] Dai, W. and Woodward, P.R., *Numerical simulations for radiation hydrodynamics. Part I: diffusion limit.* J. Comput. Phys. **142** (1998), 182-207.

[8] Pullin, D.I., *Direct simulation methods for compressible inviscid ideal gas flow.* J. Comput. Phys. **34** (1980), 231-244.

[9] Reitz, R.D., *One-dimensional compressible gas dynamics calculations using the Boltzmann equations.* J. Comput. Phys. **42** (1981), 108-123.

[10] Perthame, B., *Second-order Boltzmann scheme for compressible Euler equations in one and two space dimensions.* SIAM J. Numer. Anal. **29** (1992), 1-29.

[11] Mandal, J.C. and Deshpande, S.M., *Kinetic flux vector splitting for Euler equations.* Computers and Fluids **23** (1994), 447-478.

[12] Chou, S.Y. and Baganoff, D., *Kinetic flux-vector splitting for the Navier-Stokes equations.* J. Comput. Phys. **130** (1997), 217-230.

[13] Liu, S.H. and Xu, K., *Entropy analysis of kinetic flux vector splitting schemes for the compressible Euler equations.* ICASE Report 99-5 (1999).

[14] Jiang, S. and Ni, G.X., *A γ-model BGK scheme for compressible multifluids.* Int. J. Numer. Meth. Fluids **46** (2004), 163-182.

[15] Xu, K., Kim C., Martinelli I. and Jameson A., *BGK-based scheme for the simulation of compressible flow.* Int. J. Comput. Fluids Dynamics **7** (1996), 213-235.

[16] Xu, K., Martinelli I. and Jameson A., *Gas-kinetic finite volume methods, flux-vector splitting and artificial diffusion.* J. Comput. Phys. **120** (1995), 48-65.

[17] Cercignani, C., The Boltzmann Equation and Its Applications. Berlin, New York: Springer-Verlag, 1988.

[18] Chapman, S. and Cowling, T.W., The Mathematical Theory of Non-Uniform Gases, 3rd ed. Cambridge: Combridge Univ. Press, 1990.

[19] van Leer, B., *Towards the ultimate conservative difference schemes V. A second-order sequal to Godunov's method.* J. Comput. Phys. **32** (1979), 101-136.

[20] Xu, K., *A gas-kinetic BGK scheme for the Navier-Stokes equations and its connection with artificial dissipation and Godunov method.* J. Comput. Phys. **171** (2001), 289-335.

[21] Jameson, A., Schmidt, W. and Turkel, E., *Numerical solutions of the Euler equations by finite volume methods using Runge-Kutta time-stepping schemes.* AIAA Paper 81-1259, 1981 (AIAA Press, Washington DC).
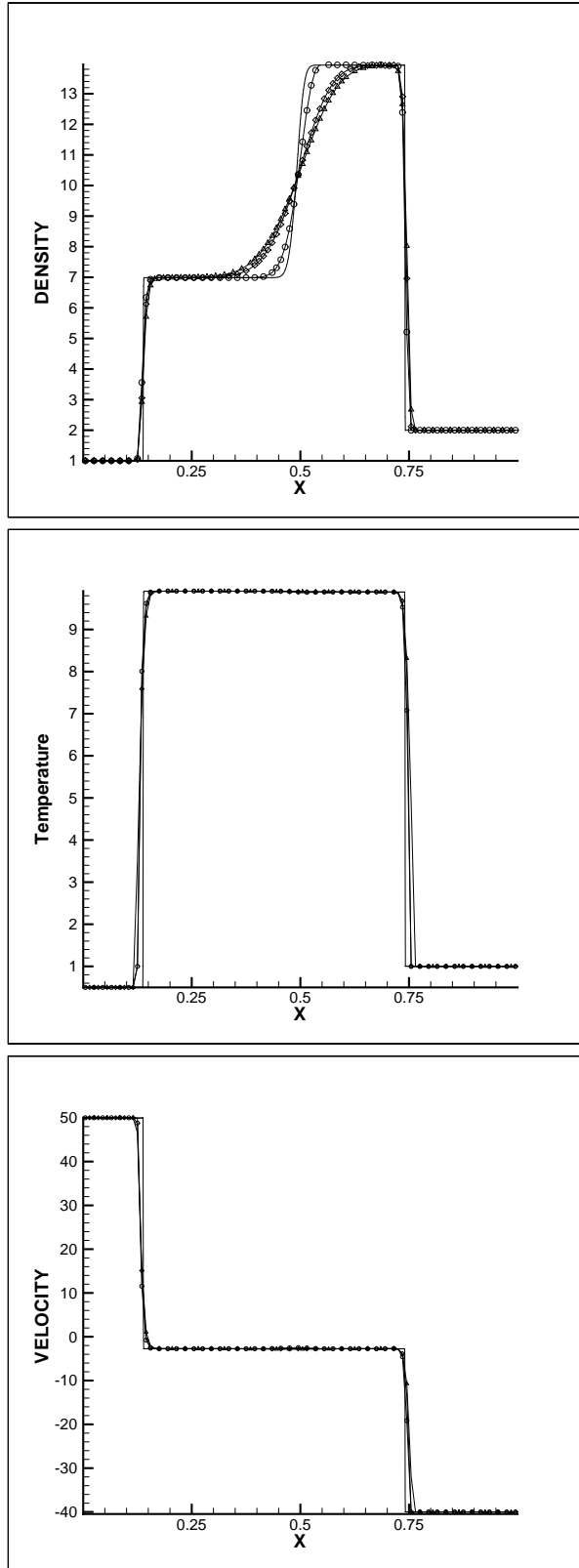
Figure 1: Solid line: the solution obtained using 2000 cells; Gradient: the 1st-order BGK scheme; RTriang: T-M's results; Diamond: the 2nd-order BGK scheme
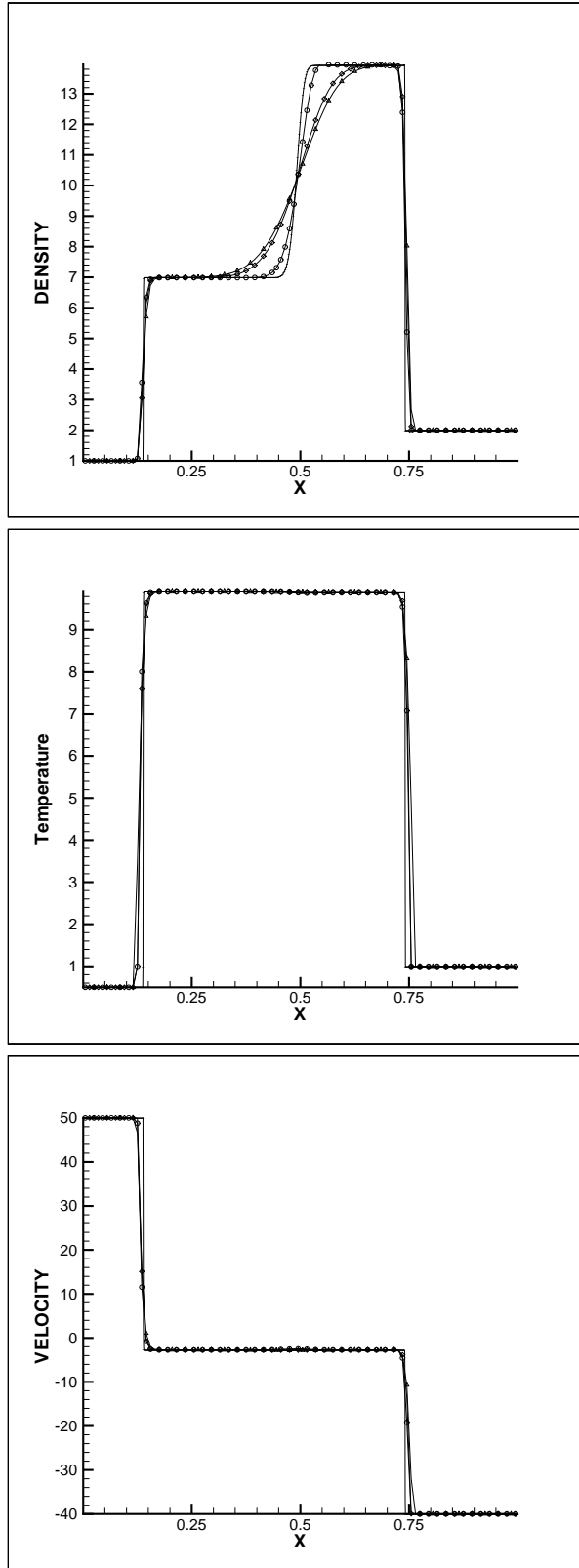
18

Figure 2: Solid line: the solution obtained using 2000 cells; Gradient: the 1st-order BGK scheme; RTriang: T-M's results; Diamond: the 2nd-order BGK scheme
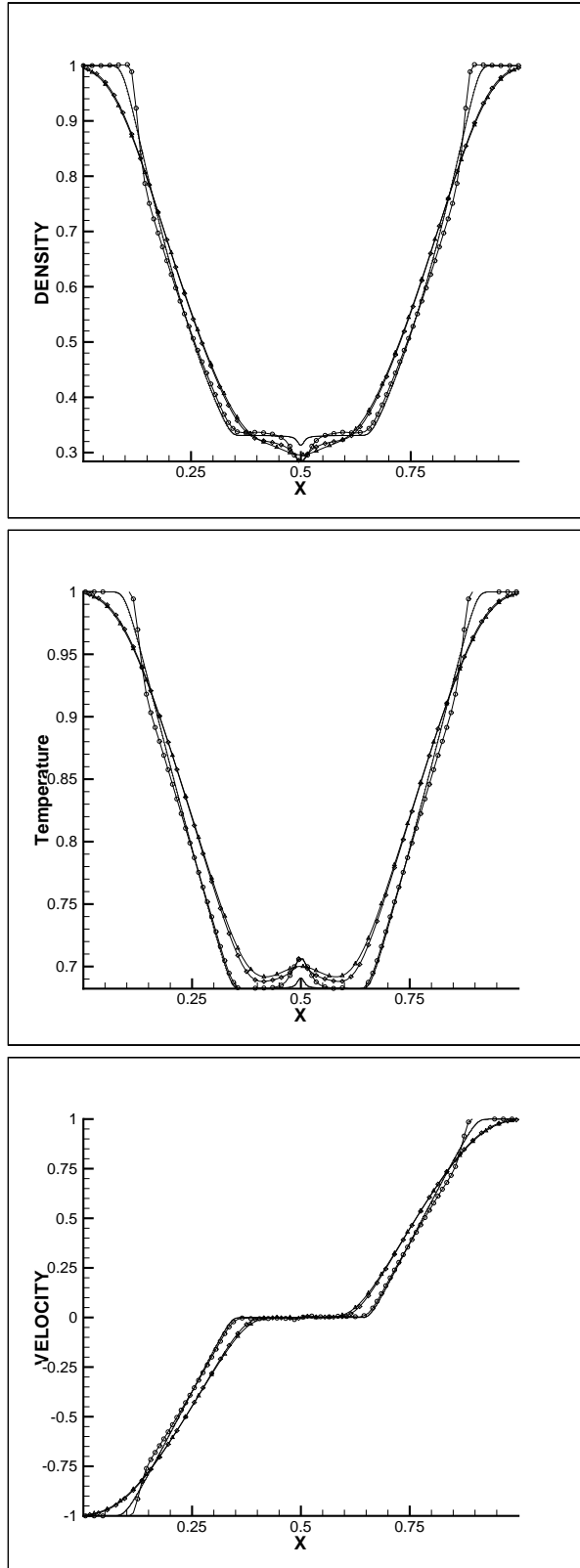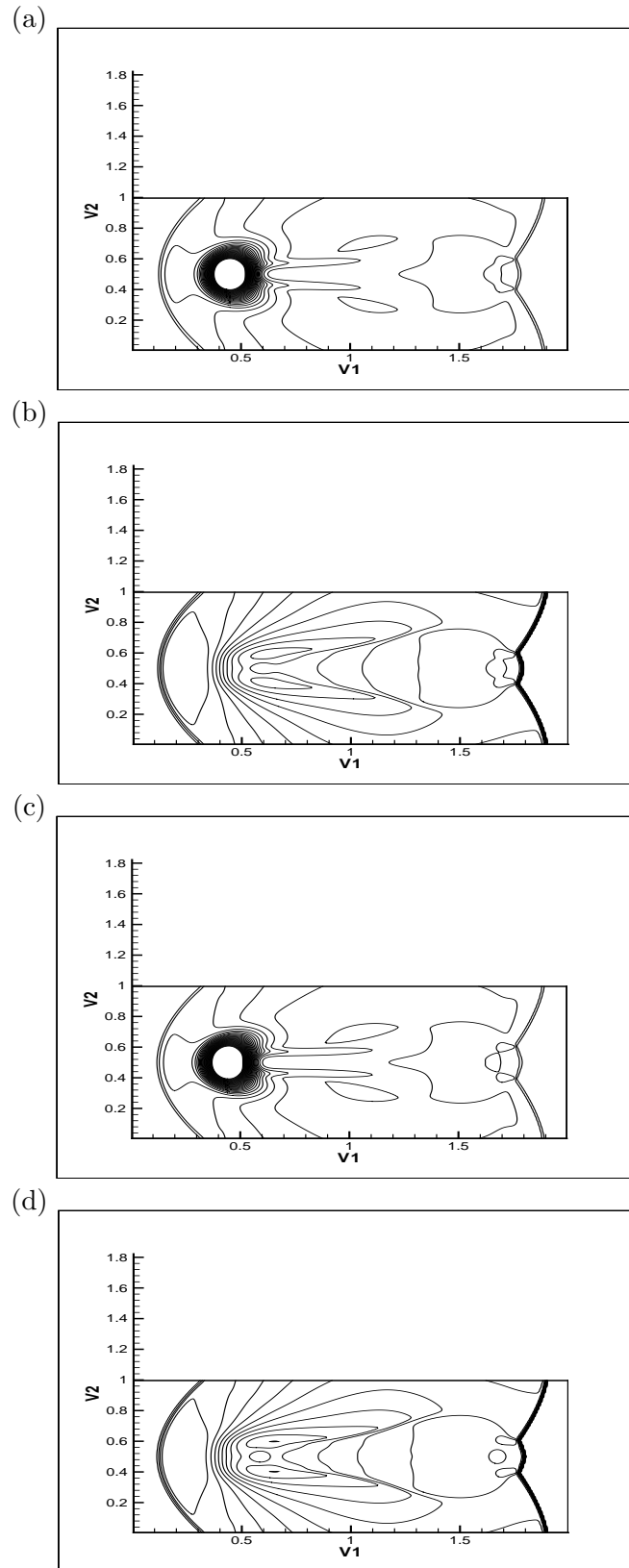
Figure 3: Solid line: the solution obtained using 2000 cells; Gradient: the 1st-order BGK scheme; RTriang: T-M's results; Diamond: the 2nd-order BGK scheme

Figure 4: The solutions obtained using 256×128 cells; (a) density and (b) temperature for the KFVS scheme; (c) density and (d) temperature for the 2nd-order BGK scheme. Temperature, 15 contours: 1.745488 to 26.1831; Density, 30 contours: 2.59141-96.4827
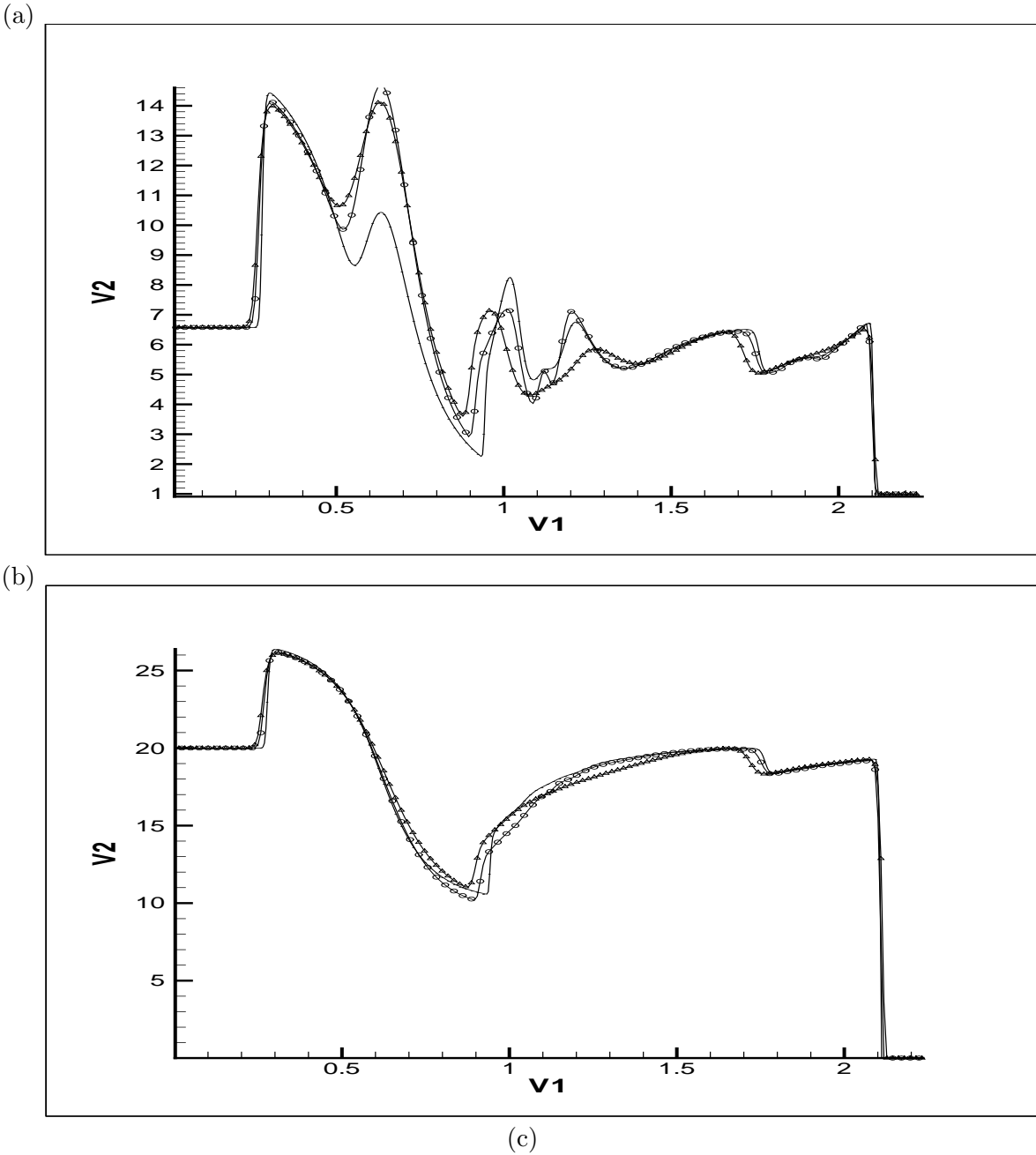
21

(a)

(b)

(c)

Figure 5: The density and temperature in the diagonal of $x = 2y$ obtained using the KFVS and 2nd-order BGK schemes in Problem 4. Square: the 2nd-order BGK scheme with 512×512 cells; Delta: the 2nd-order BGK with 256×256 cells; Diamond: the KFVS scheme with 256×256 cells
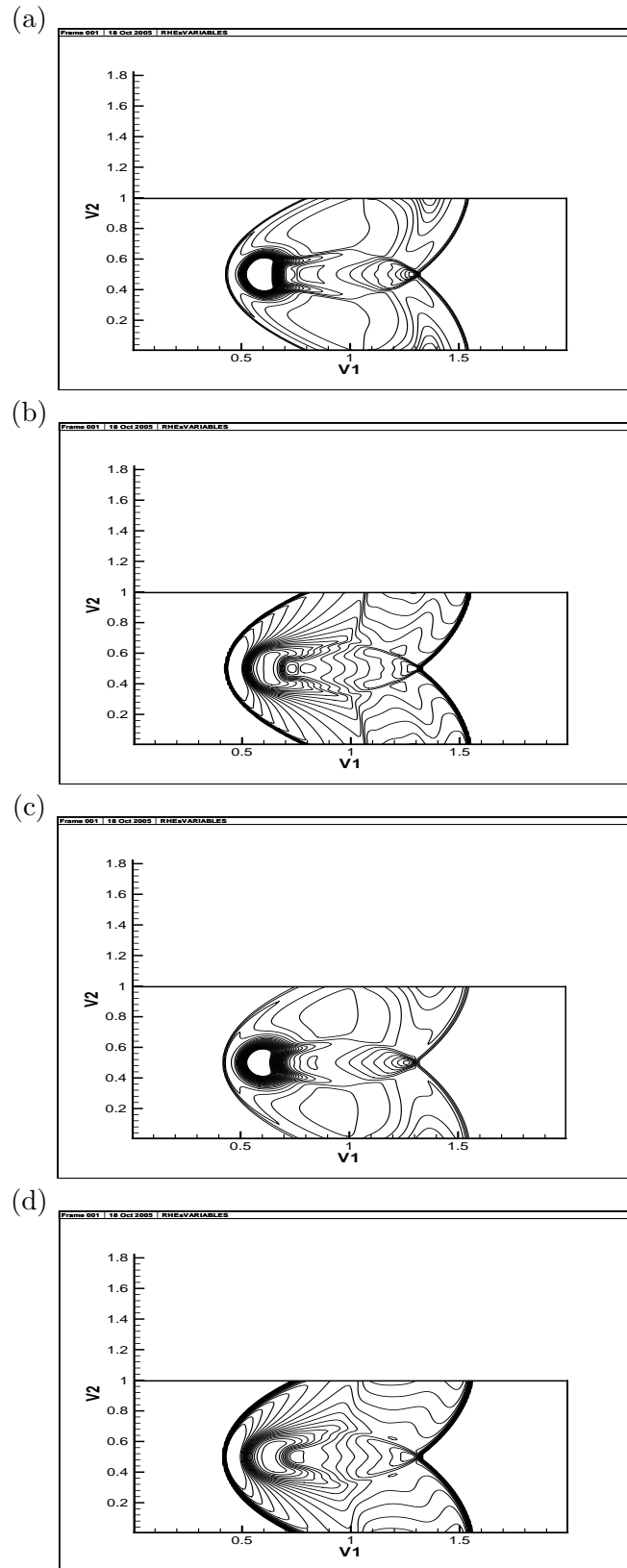
Figure 6: The results with 256×128 cells in Problem 5; (a) density and (b) temperature for the KFVS scheme; (c) density and (d) temperature for the 2nd-order BGK scheme. Temperature, 20 contours: 0.199425 to 2.2785; Density, 30 contours: 2.07753-33.326
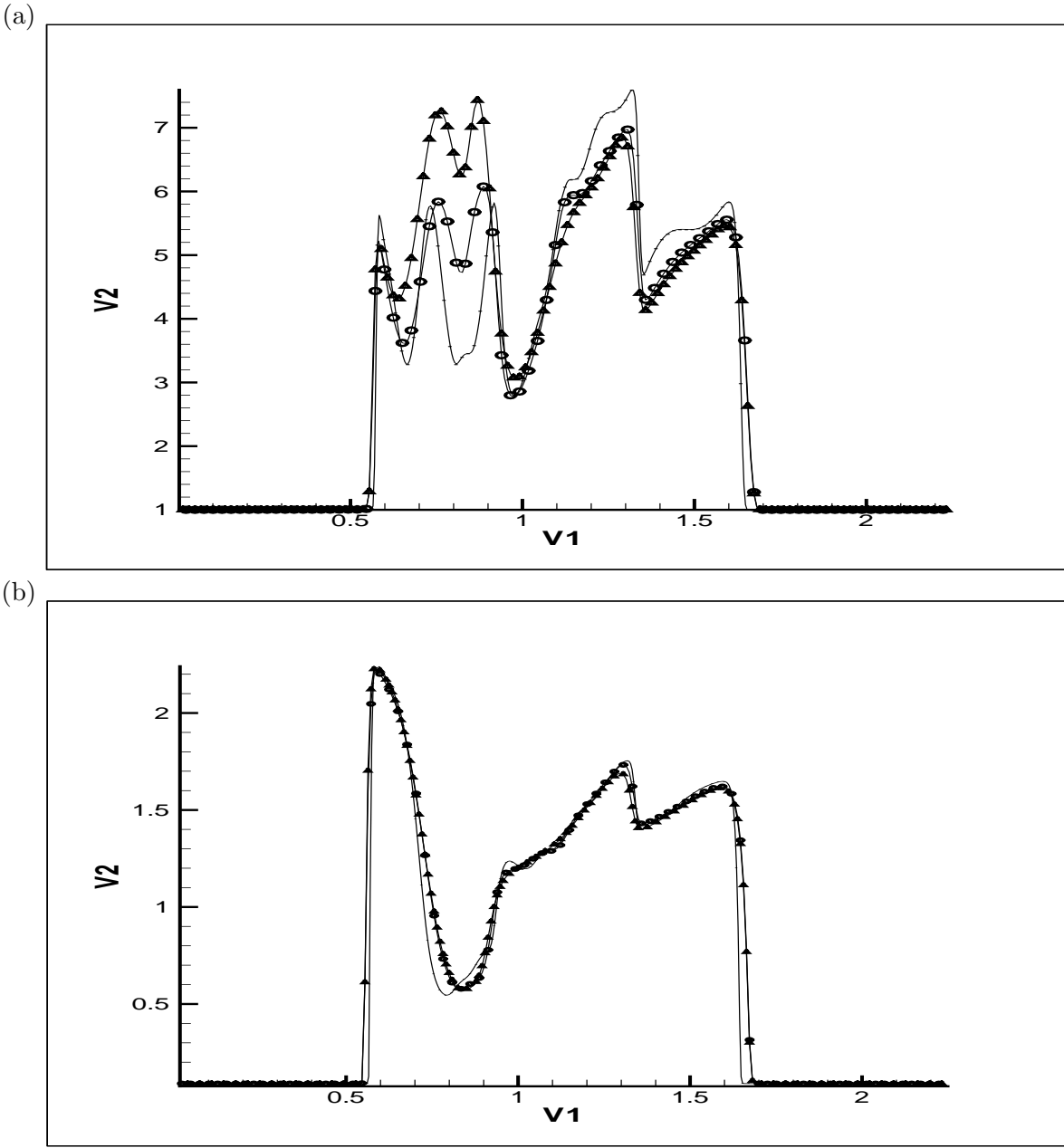
Figure 7: Density and temperature in the diagonal of $x = 2y$ using the KFVS and 2nd-order BGK schemes in Problem 5. Square: the 2nd-order BGK scheme with 512×512 cells; Delta: the 2nd-order BGK sceheme with 256×256 cells; Diamond: the KFVS scheme with 256×256 cells